

Building and Utilizing a Discrete Fracture Network Model of the FORGE Utah Site

Aleta Finnila¹, Bryan Forbes² and Robert Podgorney³

¹Golder Associates Inc., 18300 Union Hill Road, Redmond, WA 98052

²EGI, University of Utah, Salt Lake City, UT 84108

³Idaho National Laboratory, 1955 N. Fremont Ave, P.O. Box 1625, Idaho Falls, ID 83415

afinnila@golder.com

Keywords: DFN, FORGE, Milford, Utah, discrete, fracture

ABSTRACT

The Frontier Observatory for Research in Geothermal Energy (FORGE) site in Milford, Utah, is being designed as an Enhanced Geothermal System (EGS) laboratory with funding provided for the next five years to allow investigators to interactively develop and optimize EGS methodology. In preparation for this process, it is necessary to develop baseline models using Earth modeling, continuum modeling and discrete modeling methods. One of the methods employed comprises building a Discrete Fracture Network (DFN) model of the site. DFN models are particularly well suited to predicting hydraulic stimulation outcomes because they represent the pre-existing natural fracture network where much of the fluid flow is expected to occur. They can also be used to select optimal well trajectories and aid in the interpretation of well test results. This work shows the workflow used to develop the FORGE Utah DFN baseline model and suggests the potential utility of the model for use by future investigators.

1. INTRODUCTION

FORGE is a multi-year initiative funded by the US Department of Energy (DOE) for testing targeted EGS research and development. The site is located inside the southeast margin of the Great Basin near the town of Milford, Utah, and is described in detail in the Phase 2B Report (EGI, 2018a). The current Phase 2C work includes the development of baseline models using Earth, continuum and discrete modeling methods. One of the discrete models being developed is a reference DFN, the creation and potential utilization of which is documented in this paper.

The DFN incorporates measured surface and well log FORGE site data to create planer fractures that communicate as a single hydrological and mechanical system. A Formation Micro Scanner (FMI) log was obtained from well 58-32 that served as the test well during Phase 2B. The FMI data was used to develop fractures where the location and orientations are known. Fractures inferred away from direct observation are represented as stochastic populations having mean values consistent with known data. An earlier version of the DFN was created during Phase 2B which provided early analysis of the resident natural fracture sets (Forbes, et al., 2019). The Phase 2C DFN described here builds on that earlier work and adds further refinement, including the combination of both stochastic and deterministic fractures and adjustments to the fracture properties.

The DFN and subsets of the DFN will be made available to researchers and the public at the close of Phase 2C. These fracture sets will be applicable in, but not limited to: sensitivity tests, hydraulic fracturing numerical modeling, flow path analysis between wells, and the investigation of near-well effects during well testing. The DFN is also upscaled to provide continuum modelers 3D properties such as fracture porosity, directional permeability and sigma factor.

2. DFN MODEL CONSTRUCTION

The FORGE reference DFN model was constructed using FracMan software (Golder Associates, 2019). The workflow to create the DFN is subdivided into four sections: determining the boundaries of the modeling region, creating the stochastic fracture set, creating the deterministic fracture set, and fracture calibration.

2.1 Define Model Region

The DFN model region is sized to accommodate the geothermal reservoir intersected by well 58-32 and future injection and production wells along with their predicted stimulation volumes created during FORGE Phase 3. This results in a region box 2.5 km x 2.5 km x 2.75 km, located approximately between depths of 400 m to 3200 m below the surface (Figure 1a). The lithology is divided into two broadly defined units, comprising granitic basement rocks (granitoid) and the overlying basin fill sedimentary deposits. The DFN is generated only in the granitoid rock volume of the region box (Figure 1b). Temperatures in the region are predicted to be between 60°C and 250°C based on measurements in 58-32 with a temperature gradient of 70°C/km (Allis et al., 2018). The model region is rotated 25° from the N-S and E-W global coordinate frame so that the local coordinate frame is aligned with the principal horizontal stress directions as reported in the Phase 2B Final Topical Report (EGI, 2018a) with S_{Hmax} (σ_2) at N25°E and S_{Hmin} (σ_3) at N115°E (Figure 1c). This allows for easier interpretation of tensor values calculated using the local coordinate frame.

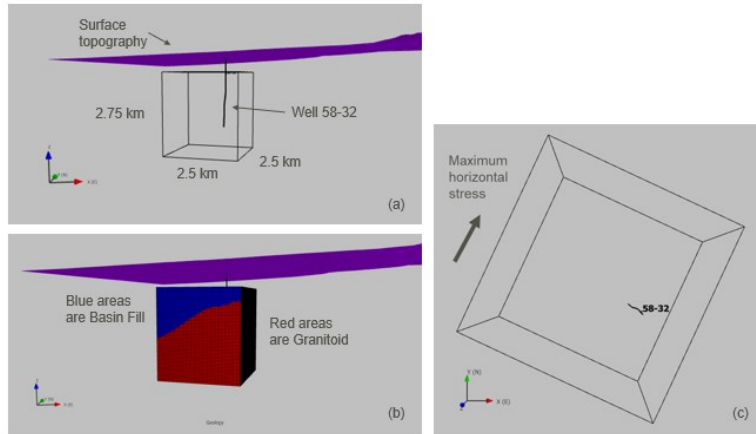


Figure 1: DFN model region showing a) location with respect to the surface and well 58-32, b) regions of basin fill and granitoid, and c) orientation with respect to the maximum horizontal stress.

2.2 Stochastic Fracture Set

Fractures in what is called the Stochastic Fracture Set are generated based on the characterized statistical properties from fractures directly observed at 58-32 and nearby outcrops of the same basement rocks.

2.2.1 Fracture Orientation

Fracture orientations for the Stochastic Fracture Set are based on the Run 1 Formation Micro Scanner (FMI) log interpretation of Well 58-32 (EGI, 2018b). Four categories of fractures were included as interpreted in the FMI log with numbers of fractures in each category shown in Figure 2.

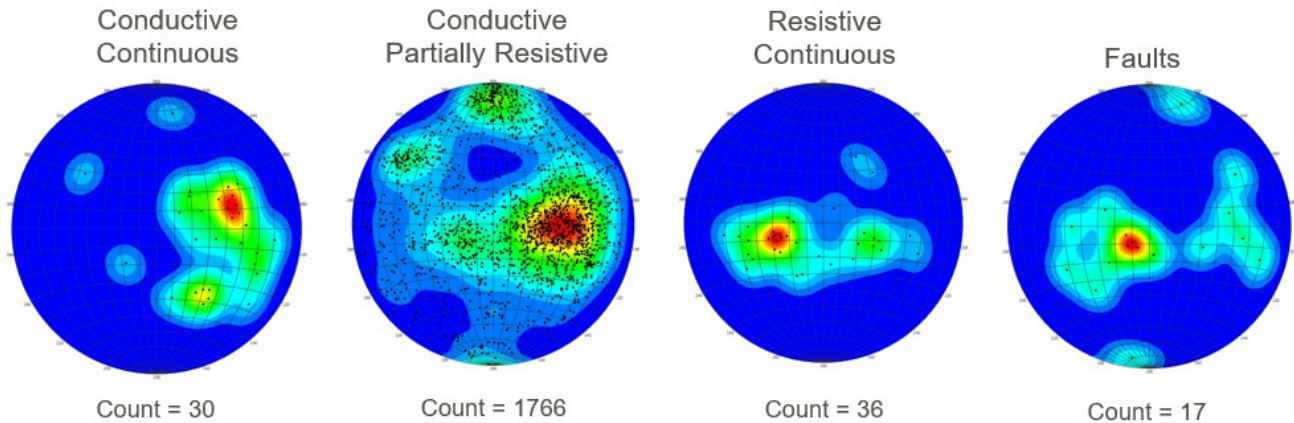


Figure 2: Count and orientation of fractures from FMI log of well 58-32 located in the granitoid bedrock (MD 1031.9 - 2295.8 m). Fracture poles are plotted in lower hemisphere, equal area stereonets and the density contours have not been weighted to compensate for the bias introduced from the well trajectory angle.

It is important to remember that the fracture population measured in a well is biased based on the relative orientation of the fractures with respect to the well trajectory angle. Well 58-32 is vertical so vertical or sub-vertical fractures are not sampled as easily as inclined or horizontal ones. When building the Stochastic Fracture Set, this bias was compensated for using a weighting factor based on Terzaghi (1965). The probability of using each measured value is adjusted in proportion to the assigned value of W :

$$W = \frac{1}{\cos \delta}, \quad \delta < 81.8^\circ; \quad W = 7, \quad 81.8^\circ \leq \delta < 90^\circ \quad (1)$$

Where δ is the angle between the well borehole and the fracture pole. A maximum value of 7 for the weighting function was imposed to account for the finite well radius (Mauldon and Mauldon, 1997). The FMI fracture orientations shown both as measured and as adjusted to account for the bias caused by the well trajectory are shown in Figure 3.

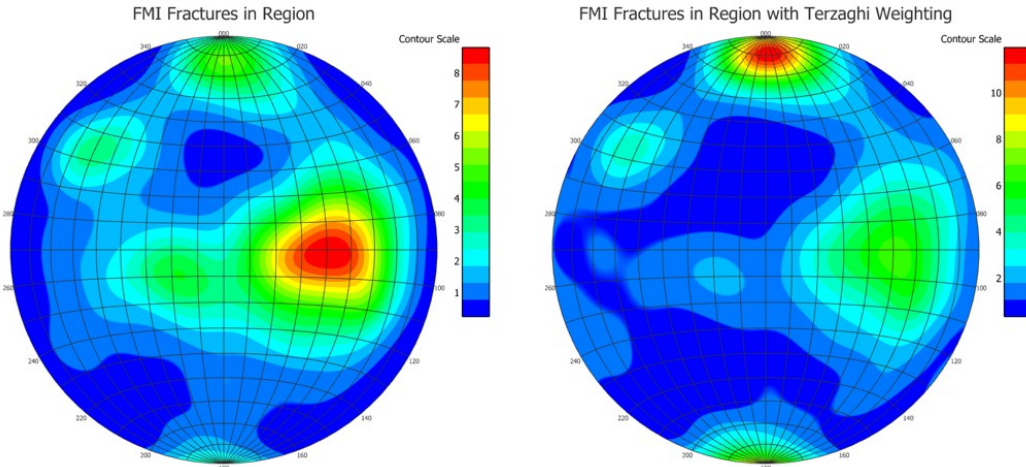


Figure 3: Contour plots of 58-32 FMI fracture poles in lower hemisphere, equal area stereonets showing the relative intensities before bias correction (left) and after applying Terzaghi weighting (right).

In addition to the FMI data from well 58-32, there has been extensive mapping of fracture trace lengths and orientations in the nearby Mineral Mountains where the target granite from the FORGE reservoir is exposed (Coleman, 1991; EGL, 2016; Bartley, 2018). Orientation data from four of these locations is shown in Figure 4. These locations are approximately 5 miles from the FORGE site (Figure 5).

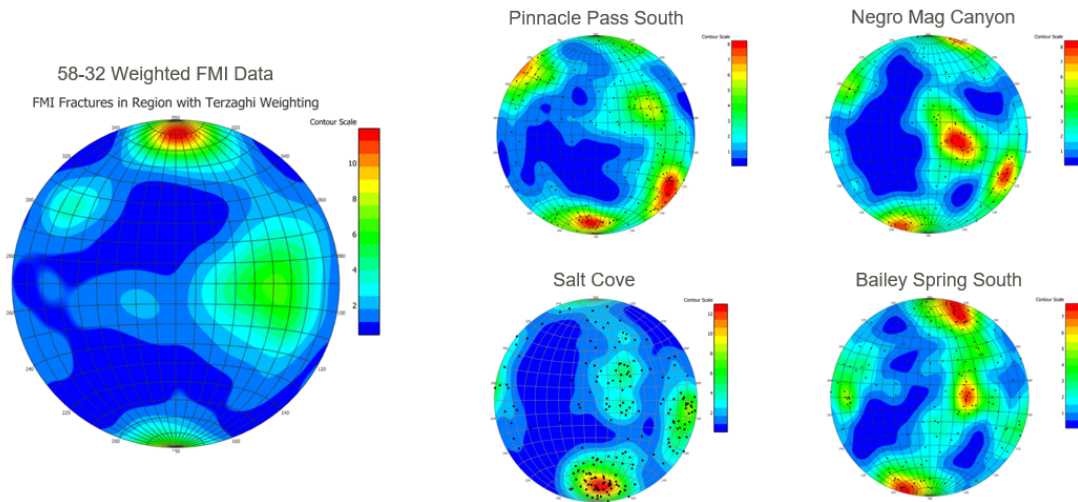


Figure 4: Contour plots of fracture poles in lower hemisphere, equal area stereonets comparing the weighted FMI data for 58-32 on the left with four outcrop areas located in the nearby mountains on the right.

As described in Bartley (2018), the Miocene granitic rocks in the northern half of the Mineral Mountain range all contain a similar fracture pattern. The pattern includes three fracture sets in the following general orientations: E-W to WNW-ESE striking and subvertical; NE-SW to NNE-SSW striking and steeply dipping; and gently W-dipping with strikes that vary from NW to N to NE. In some areas, two of the concentrations of poles to fractures that define the three sets merge into a girdle, but the overall pattern remains the same. In the areas which are located nearest to the FORGE area, steep E-W striking fractures form the most abundant and continuous set. The E-W fractures commonly bound the steep NE-striking and gently west-dipping fracture sets. As with the fracture orientations in the outcrop data, well 58-32 also shows three fracture sets with the most prominent being a subvertical E-W striking set. The two other sets include a moderately dipping N-S set and more steeply inclined NE-SW striking set.

Since generated fracture orientations in the Stochastic Fracture Set were created using a bootstrapping method on the measured values in 58-32, these individual sets did not need to be described using set percentages or mean orientation values. This collection of measured

data is used to determine similar populations where a Fisher concentration value controls how exactly the resulting orientations align with the original data set. A Fisher concentration value of “50” was used to closely, but not exactly match the measured FMI orientation data set in the Stochastic Fracture Set. Use of the bootstrap method has advantages including ease of implementation and not needing to rely on accurate descriptions of individual fracture sets, e.g. how many, relative proportion of each set, parametric fits for each set, etc. A limitation, however, is that there can only be one size relationship used for all the fracture population and no termination rules can be imposed with one set preferentially terminating against another set.

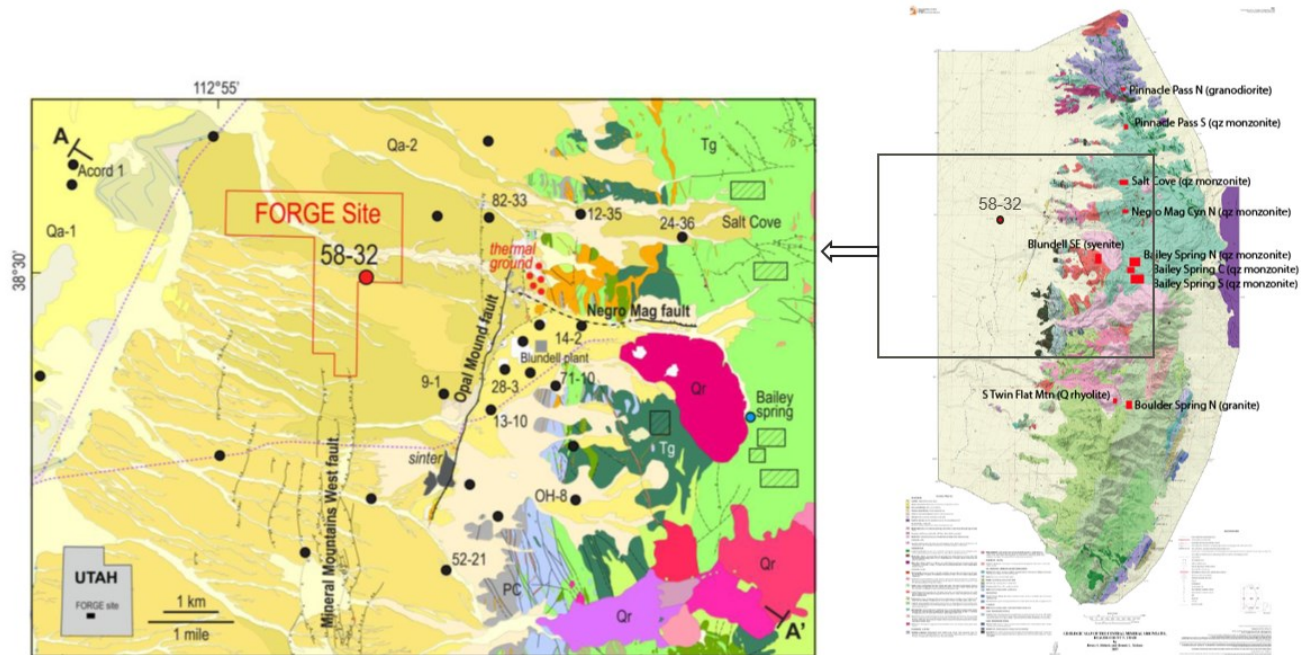


Figure 5: Locations of FORGE site and outcrop mapping locations on geologic maps. Close-up map on left from EGI (2018a) and map on right from Sibbett and Nielson (2017).

Figure 6 shows a sequence of contoured stereonet. The first on the left is the raw FMI data from 58-32. The next shows the weighted concentrations of fracture pole orientations which were used to generate the Stochastic Fracture Set shown in the third stereonet. The final stereonet on the right shows the orientations of the fractures in the Stochastic Fracture set which intersect 58-32. It is apparent from the similarity in the first and last stereonets that the agreement between the measured values and those generated in the Stochastic Fracture Set of the DFN is very good.

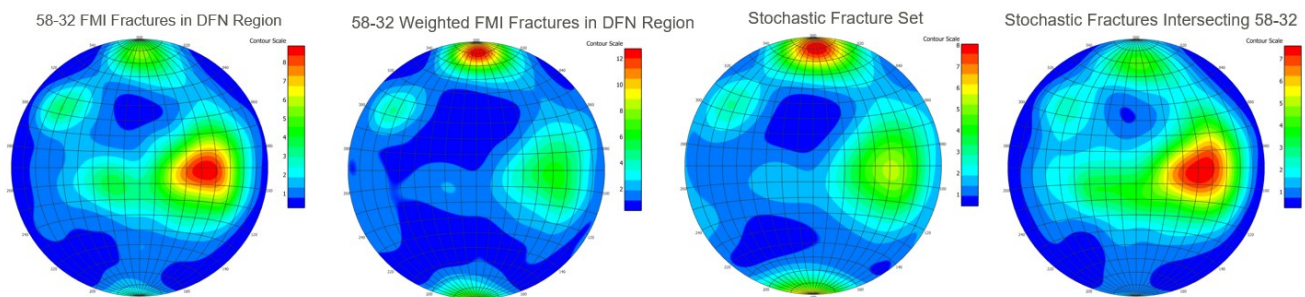


Figure 6: Contour plots of fracture poles in lower hemisphere, equal area stereonets comparing the generated Stochastic Fracture Set orientations with measured FMI data from 58-32.

2.2.2 Fracture Size and Shape

Fracture size for the Stochastic Fracture Set was estimated using trace length data from the nearby outcrops in the Mineral Mountains from the same geologic unit as is present at the FORGE site. The trace length data fit log-normal distributions (Figure 7) with mean and standard deviations shown in Table 1.

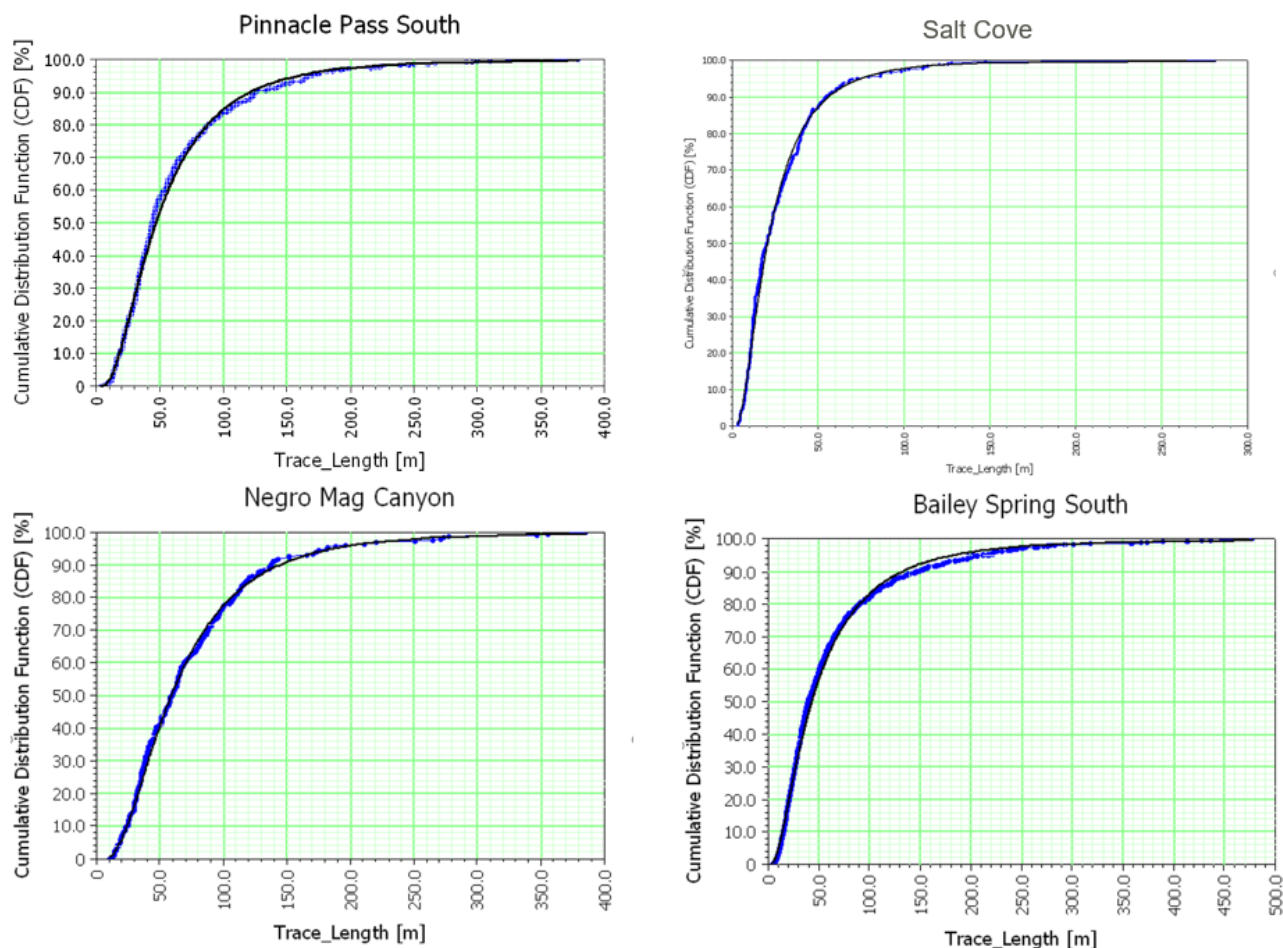


Figure 7: Log Normal fits to trace length data from outcrops in the Mineral Mountains. Trace lengths were measured from digitized 2D maps from the work of Bartley (2018) and Colman (1991).

Table 1: Log Normal distribution parameters for trace length data from the Mineral Mountains.

	Mean [m]	Std Dev [m]
Pinnacle Pass South	61.8	52.2
Salt Cove	27.6	23.9
Negro Mag Canyon	75.3	59.3
Bailey Springs South	63.4	66.3
Average	57.0	50.4

Measured values fitting a log-normal distribution often represent data sets which are actually present in a power law distribution: power law distributions that are truncated at both the low and high ends of the range appear as log-normal. In order to investigate this possibility, trace lengths were plotted on a log-log plot of the area normalized complementary cumulative number vs the trace lengths (Figure 8). Sections of these curves which plot as straight lines on this plot are following a power law distribution with the absolute value of the slope of the line indicating the exponent of the power law distribution. Deviations from this straight-line show truncation effects of the measurement technique.

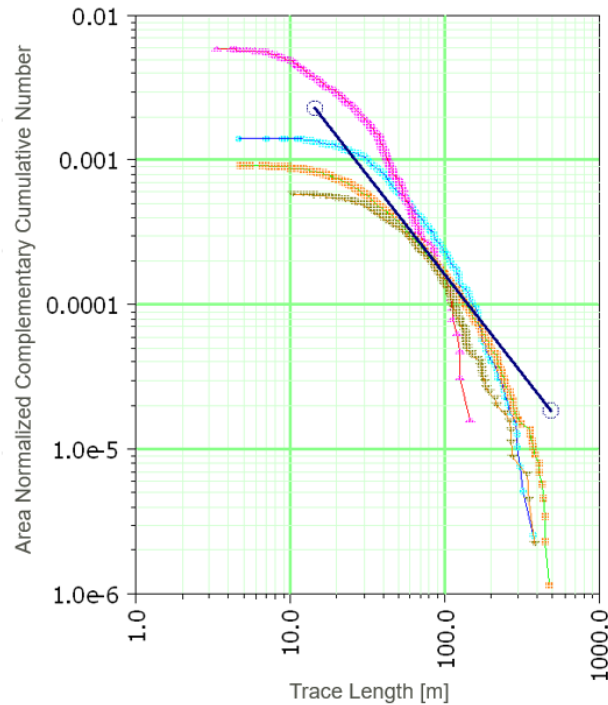


Figure 8: Power law fit to outcrop trace length data: Pinnacle Pass (blue), Salt Cove (pink), Bailey Negro Mag Canyon (brown), and Spring South (orange).

While there are some straighter lines in trace length values between approximately 30 m and 110 m, the slopes between the different outcrops range from -1.3 to -1.9 which is a pretty large range. Generally, multiple data sets spanning different magnitudes of fracture sizes are necessary to accurately define a power law relationship. These different data sets could include measured apertures in photomicrographs prepared from core samples for very small fracture sizes to large fault lengths cataloged in the region. Until more work is done to further investigate a power law relationship for the fracture sizes found in the FORGE site, a log-normal size distribution is assumed. The reference FORGE DFN described in this paper uses a log-normal fracture size parameterization using the average mean and standard deviations found from the four outcrop data sets (Table 1).

A DFN built using a power law distribution for fracture size would have many, many more small fractures than a DFN built using a log-normal fracture size distribution. These very small fractures are often not explicitly generated in the DFN, but their absence is compensated in different ways depending upon the parameterization method used. This reference DFN uses a minimum size cutoff of 10 m for the equivalent radius (R_e) of the fracture and a maximum size cutoff of 150 m. The R_e of a fracture is defined as the radius of a circle having the same fracture area as the actual fracture (which may not be circular). For example, a circular fracture having a R_e of 10 m can create a trace length of 0-20 m while a fracture having a R_e of 150 m can create a trace length between 0-300 m.

Fracture shapes are assumed to be roughly circular and are represented in this reference DFN as six-sided polygons. Polygonal fractures such as the six-sided ones used in the reference DFN can have slightly higher maximum trace lengths than the $2xR_e$ of the circular fractures.

2.2.3 Fracture Intensity

The best source of fracture intensity in the FORGE reservoir region comes from the lineal fracture intensity, P_{10} , measured from the FMI log data. P_{10} is defined as the number of fractures per unit of length. On a Cumulative Fracture Intensity Plot (CFI), the slope of the line shows the inverse of the P_{10} value; so higher slopes correspond to lower fracture intensities. Combining the four types of FMI fractures that were used for the fracture orientation analysis, there are 1849 fractures in the granitoid. With the well penetrating approximately 1264 m into the granitoid bedrock, the P_{10} value for the full interval is 1.46 1/m (1849/1264). Looking at the CFI plot for 58-32, however, it appears that there are two distinct regions of fracture intensity: a shallower region extending from the top of the granitoid to a MD on the well of approximately 1300 m having higher lineal fracture intensity, and a deeper region extending to the bottom of the well having a lower lineal fracture intensity (Figure 9). This seems to correspond to the transition from the Monzodiorite to the Monzonite lithology where the bulk porosity also drops correspondingly (Figure 10). As the FORGE site is primarily investigating the potential for exploitation at deeper, hotter zones, the choice was made to use a single fracture intensity value corresponding to the deeper zone where the P_{10} is 1.18 1/m. A future refinement of the reference DFN might divide the granitoid into shallower and deeper zones with varying fracture intensities.

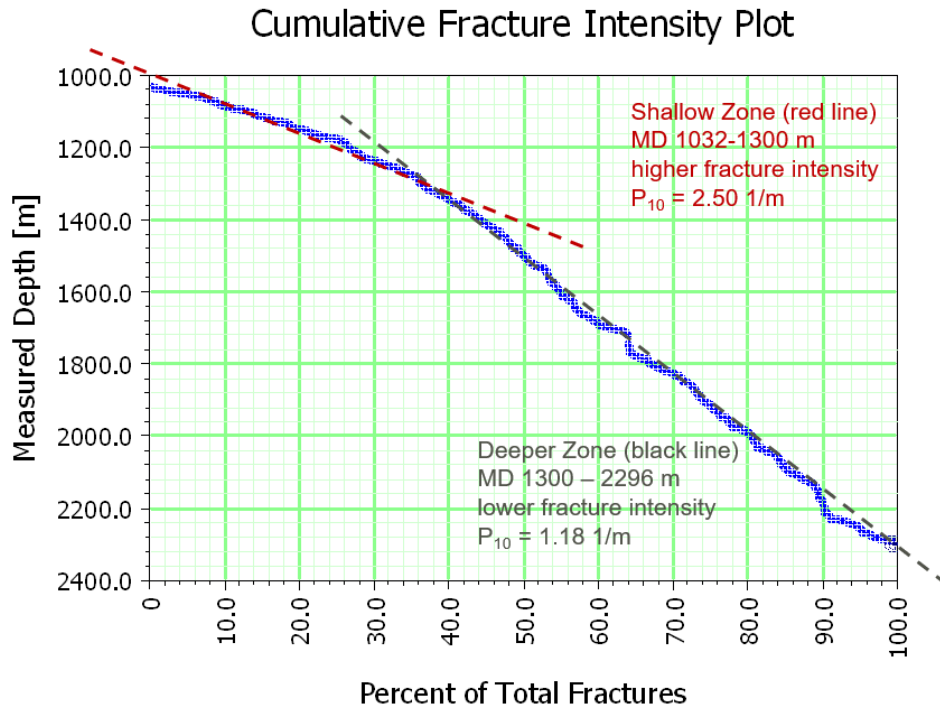


Figure 9: CFI plot of 58-32 FMI fractures in granitoid.

In order to generate the correct fracture intensity for the Stochastic Fracture Set, fractures are added to the model until the correct number are intersecting the well in the specified interval. For this to be an effective method, the orientations of the generated fractures must accurately reflect the populations measured in the well.

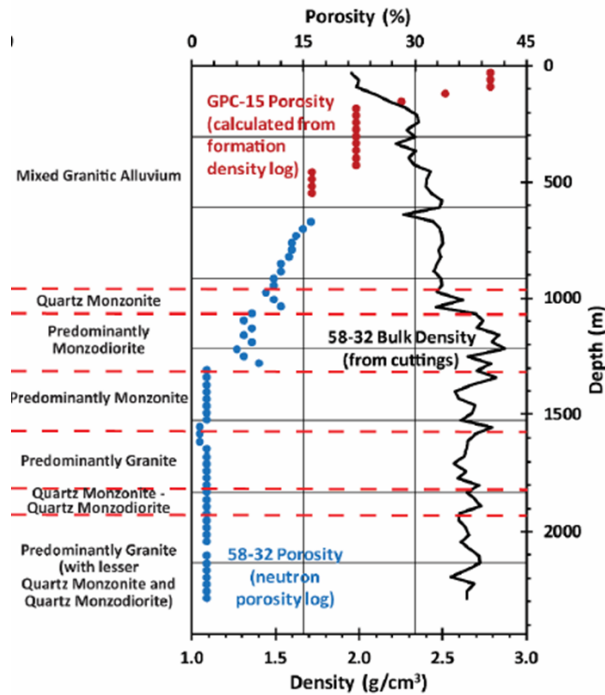


Figure 10: Measured density values from drill cuttings at 100-foot intervals in well 58-32 (Gwynn et al., 2018).

2.2.4 Clipping to Granitoid Surface

Once the fracture geometric properties such as orientation, size, shape and intensity are defined for the Stochastic Fracture Set, the fractures are generated within the model region. Because the model region extends above the bedrock reservoir, a clipping step is performed to

remove any fractures above the granitoid surface (Idaho National Laboratory, 2018). Fractures that intersect this surface are trimmed to remove parts that lie above, while retaining the parts that lie below. After clipping, there are approximately 2.9 million fractures in the Reference DFN.

2.3 Deterministic Fracture Set

While a stochastic set of fractures is helpful for estimating unknown fracture populations, we would like the DFN to honor the locations and orientations of the fractures that have been measured in the FMI log. These will be generated in a separate set called the Deterministic Fracture Set. Stochastic fractures intersecting 58-32 in the DFN will be removed so that a synthetic well log created from the trajectory of 58-32 in the DFN will look identical to the actual one. While this fracture set is deterministic in the sense that the general fracture locations and orientations are known to some extent, the fracture sizes, shapes and exact locations of the centers of the fractures are still randomly generated, so that different realizations of the fracture set are also possible.

2.3.1 Remove Stochastic Fractures Intersecting Well

There were 1510 fractures from the Stochastic Fracture Set intersecting 58-32. This number will remain constant regardless of the random seed used during fracture generation as the algorithm for creating these fractures uses a P_{10} value to constrain fracture intensity. The actual location, size and orientation of these Stochastic Fracture Set fractures will vary if new seed numbers are used to generate other realizations. Note that this number, 1510, is less than the number of fractures intersecting 58-32 in the granitoid (1849). The Stochastic Fracture Set uses the deeper zone P_{10} value for fracture intensity throughout the DFN region, so the target number of intersecting fractures is correspondingly lower.

2.3.2 Generate Deterministic Fracture Set

At each depth identified in the FMI log of 58-32, a fracture is generated that intersects that location and has the orientation as interpreted in the FMI log. The intersection with the well is not the center of the fracture, just a random point located somewhere on the fracture plane. Since the sizes of the fractures is not known, the size will be randomly generated based on the size distribution found in the stochastic intersecting fractures that have been removed from the DFN, so that the total fracture area in the DFN is not changed much by this substitution. For the Reference Set Realization, the fracture sizes followed a Normal distribution having a mean of 85.2 m and a standard deviation of 34.9.

2.4 Fracture Calibration

2.4.1 Fracture Aperture

While fracture apertures have not been measured in the core or image log data, the DFN fracture apertures can be roughly calibrated by considering the bulk rock porosity measured to be between 1-2% at reservoir depths (Figure 10) and by assuming a relationship between the aperture and the fracture size. The bulk porosity is a combination of the fracture porosity and the matrix porosity and so is an upper bound on the fracture porosity. Lab measurements of porosity from core samples was less than 0.5% (McLennan et al., 2018). When upscaling a DFN, the fracture porosity, ϕ_F , is given by:

$$\phi_F = \frac{\sum A_F e}{V_C} \quad (2)$$

Where A_F the fracture area in a grid cell, and e , the fracture aperture, get multiplied together for each fracture in a grid cell and summed while V_C is the grid cell volume. For this calibration, we assume that the aperture is linearly related to the square root of the fracture R_e :

$$e = a\sqrt{R_e} \quad (3)$$

Where a is some constant yet to be determined. This relationship is often useful in a DFN where fractures are treated as planar features having a constant aperture. In order to account for the reduced flow through rough fracture surfaces and channeling, the idealized cubic law between aperture and fracture size is reduced to a square law. This aperture may be more correctly described as a hydraulic aperture. The procedure to find a constant value for “ a ” that makes the DFN fracture porosity somewhat less than the measured bulk porosity is to simply try a value once the DFN has been generated to set an initial value for all the apertures, upscale the DFN to determine the mean fracture porosity in the rock, and then adjust the constant value until a reasonable fit is found. Using this method, a constant value of 3.0×10^{-4} yielded a mean fracture porosity of 0.46% with aperture values ranging from 0.95 mm to 3.67 mm.

One caveat to this workflow is that the reference DFN truncates fracture sizes using a minimum R_e value of 10 m so that smaller fractures are not included. How much total fracture porosity is lost through this procedure can be calculated based on the parameterization used for fracture size. The log-normal distribution utilized for the FORGE DFN doesn’t lose much porosity from this truncation, so no compensation is needed (Figure 11). If the parameterization switches to a power law distribution in the future, then the lost fracture porosity becomes significant and this would need to be considered.

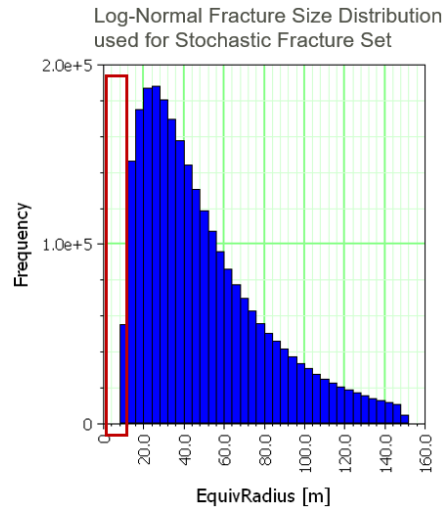


Figure 11: Bar plot of fracture sizes from the Stochastic Fracture Set with the truncation at minimum size 10 m shown.

2.4.2 Fracture Compressibility

Fracture compressibility, C_F , is calibrated from the measurements of Young’s Modulus, E , and Poisson’s Ratio, ν , performed in Phase 2B of FORGE (Figure 12). The Bulk Compressibility, C_B , is defined as:

$$B_C = \frac{3(1-2\nu)}{E} \tag{4}$$

Using E equal to 4.5×10^{10} Pa and ν equal to 0.25, the BC is 3.3×10^{-5} 1/MPa. When upscaling from a DFN, the BC is defined as:

$$B_C = C_F * \phi_F \tag{5}$$

Where ϕ_F is the fracture porosity. Since the fracture apertures have already been calculated, the fracture porosity can be determined through upscaling the DFN. Combining equations 4 and 5 then yields a mean fracture compressibility of 7.2×10^{-3} 1/MPa.

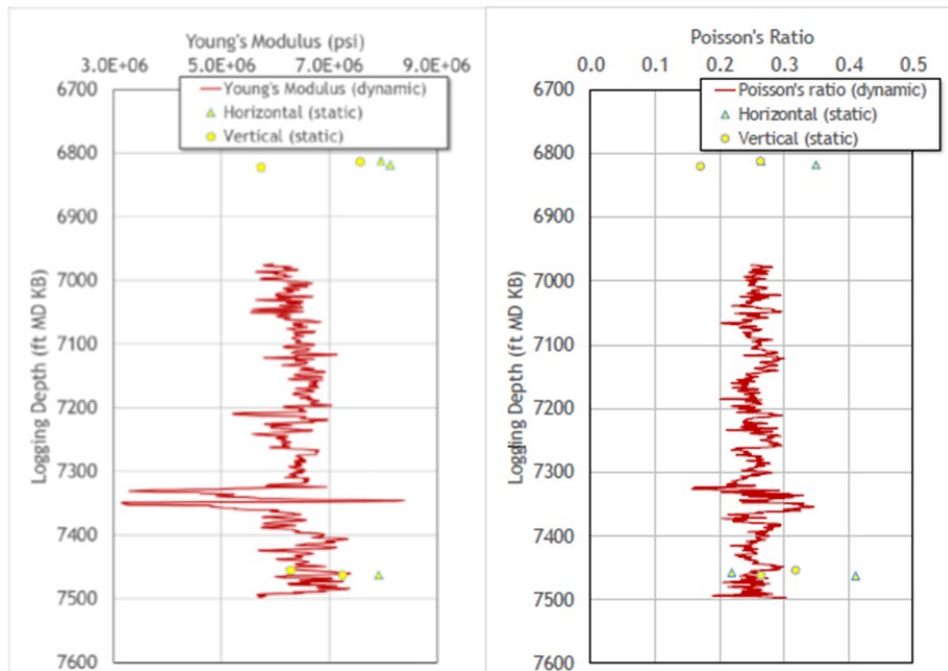


Figure 12: Logging predictions and laboratory measurements of Young’s modulus (left panel) and Poisson’s ratio (right panel). Note that the laboratory measurements were carried out on vertically and horizontally plugged samples from the cores recovered at two depths in the well. (Moore et al., 2018).

2.4.3 Fracture Permeability

The average rock in-situ permeability of the granitoid is estimated to be $4.7 \times 10^{-17} \text{ m}^2$ from well testing performed in Phase 2B (McLennan et al., 2018). In a similar workflow as was utilized to estimate fracture apertures, a relationship between fracture permeability k_F , and aperture, e , is assumed:

$$k_F = be^{1.5} \quad (6)$$

Where b is a constant that needs to be empirically determined. Using a value of b equal to 3.13×10^{-15} for the fractures in the reference DFN yields permeabilities in the cell coordinate directions IJK of $4.6 \times 10^{-17} \text{ m}^2$, $4.6 \times 10^{-17} \text{ m}^2$, and $4.9 \times 10^{-17} \text{ m}^2$ respectively.

3. DFN SUBSETS AND APPLICATIONS

With almost 3 million fractures in the Reference DFN, it can be useful to provide various subsets depending upon the purpose. Some common subsets are to filter the fractures by size to only consider the largest ones, or to perform a critical stress analysis on them and only select the ones which show high values of critical stress. In both cases, it is generally assumed that these subsets will include the most hydraulically significant fractures and only those that are connected to the well(s) of interest are included.

3.1 Subsets of the Reference DFN

One subset of the DFN includes all the fractures intersecting the well (the Discrete Fracture Set) as well as all the connected stochastic fractures having a R_e greater than 140 m (Figure 13a). This results in a set of fractures numbering approximately 15 thousand which should be amenable to hydraulic fracturing or flow simulations using finite element or discrete element modeling. Maintaining all of the fractures intersecting the well, regardless of size, ensures adequate connectivity with the well.

Another useful subset includes fractures within a 5 m radius of well 58-32 for a short 10m segment along the length of the well for use in investigating near-well effects during well testing (Figure 13b). The Reference DFN, however, is not the best source for such a subset as it has been developed to cover larger scale effects over a much larger volume and has therefore restricted fracture sizes to be at least 10 m R_e . For investigations covering much smaller volumes, some modified DFNs can be generated which allow for smaller fracture sizes.

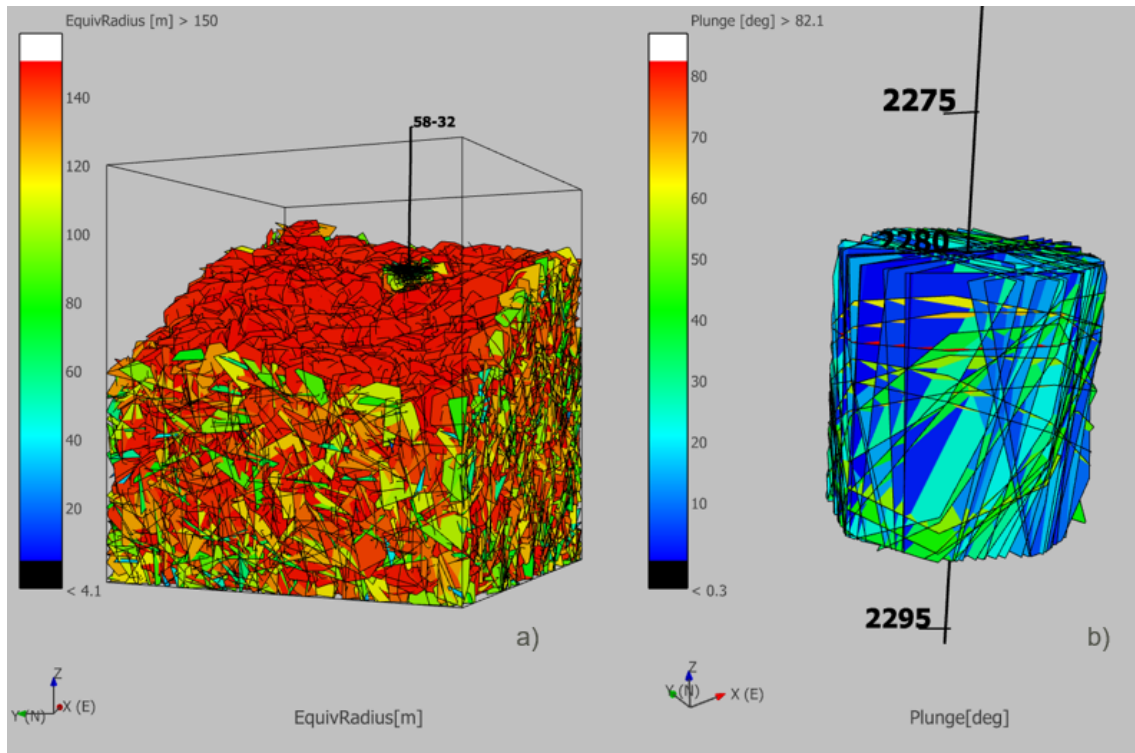


Figure 13: Subsets from the Reference DFN: a) subset containing the largest fractures and those intersecting well 58-32 with fracture color corresponding to the fracture size (equivalent radius), and b) fractures within a 5 m radius of 58-32 (clipped at the limit) over the MD 2280-2290 with fracture color corresponding to the fracture pole plunge m.

Once proposed wells are added to the model, such as an injection or production well, then various fracture pathways can be extracted that connect the wells, such as those including the fewest number of fractures or the highest conducting fracture pathway. These subsets would have tens to hundreds of fractures.

3.2 Upscaling the DFN

In order to assist continuum modeling, the DFN is also upscaled to provide bulk rock values for such parameters as porosity, directional permeability, and sigma factor (Figure 14). The properties can be averaged over varying length scales as needed. These properties can be transferred to other simulators using grid file formats or point data having associated mean property values. Other bulk rock mechanical properties such as RQD, GSI, RMR89, Young's Modulus tensors, and fracture stiffness can be generated as well.

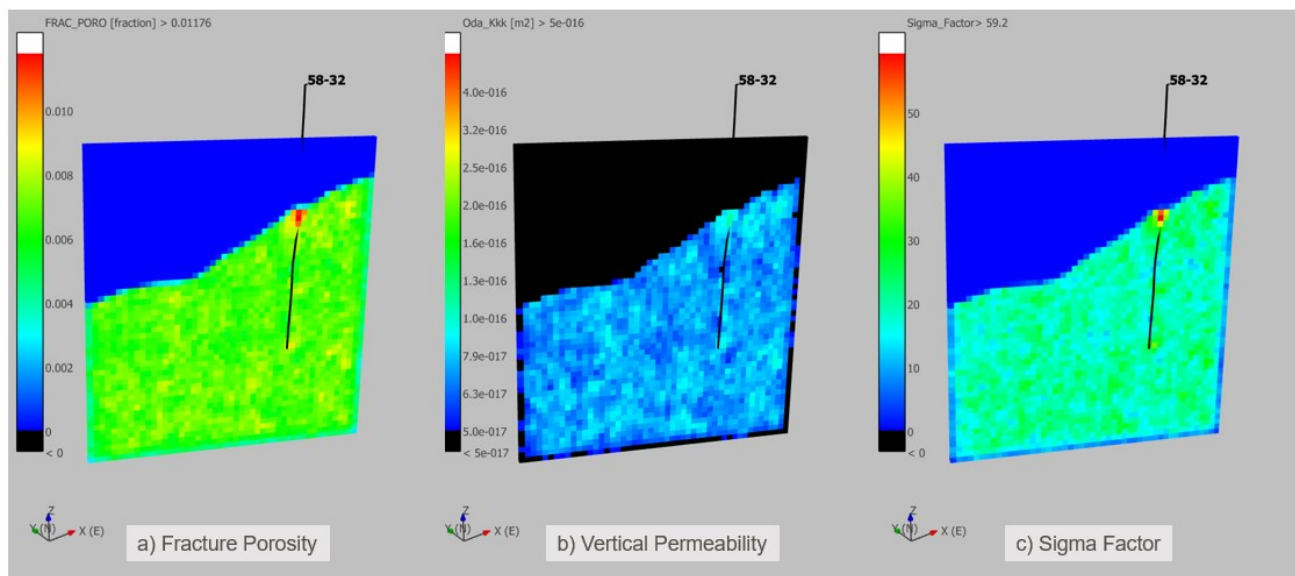


Figure 14: Upscaled property values through a slice of the model region looking to the North-Northeast.

The higher fracture intensity measured in the FMI log at shallow basement depths is captured by the DFN as shown in Figure 14a with higher local porosity and Figure 14c with higher sigma factor values representing closer fracture spacing. The orientation of these shallow fractures is less vertical than other fractures along the well as seen in the relatively lower vertical permeability visible in Figure 14b.

4. CONCLUSION

This paper describes the construction of a reference DFN for FORGE Phase 2C that is ready to be used in other Phase 2C modeling work. Subsets of the DFN have been created to provide the most significant fractures for various modeling uses. The smaller number of fractures in these subsets allows them to be used in a wider variety of modeling tools. Planned future modeling activities utilizing the DFN include interval identification for well tests, well placement studies, reservoir stimulation, and prediction of induced seismicity during operating conditions.

Additionally, other equivalent realizations of the reference DFN may be generated to measure the uncertainty in the model. Multiple DFN realizations are crucial in assessing the effect of fracture variability on completions and reservoir production. The presented reference DFN will be updated at the end of Phase 2C activities to incorporate any newly acquired data. Likely areas of change to the reference DFN include minor adjustments to fracture intensity, fracture size parameterization, and fracture property calibration.

ACKNOWLEDGEMENTS

Funding for this work was provided by the U.S. DOE under grant DE-EE0007080 “Enhanced Geothermal System Concept Testing and Development at the Milford City, Utah FORGE Site”. We thank the many stakeholders who are supporting this project, including U.S. DOE Geothermal Technologies Office, Smithfield (Murphy Brown LLC), Utah School and Institutional Trust Lands Administration, and Beaver County as well as the Utah Governor’s Office of Energy Development.

REFERENCES

- Allis, R., M. Gwynn, C. Hardwick, W. Hurlbut, and J. Moore: Thermal Characteristics of the FORGE site, Milford, Utah, FORGE Utah Technical Report, Report to Department of Energy, Geothermal Technologies Office, April 2018, (2018).
- Bartley, J. M.: Characterization of fractures in the Mineral Mountains, Technical Report, Report to Department of Energy, Geothermal Technologies Office, April 2018, (2018).
- Coleman, D.S.: Geology of the Mineral Mountains batholith, Utah [unpublished Ph.D. dissertation]: University of Kansas, Lawrence, Kansas, (1991), 219 p.
- Energy and Geoscience Institute at the University of Utah: Roosevelt Hot Springs, Utah FORGE Final Topical Report 2018 [data set]. Retrieved from <http://gdr.openet.org/submissions/1038>, (2018a).

Finnila et al.

- Energy and Geoscience Institute at the University of Utah.: Roosevelt Hot Springs, Utah FORGE Well 58-32 Schlumberger FMI Logs DLIS and XML files [data set]. Retrieved from <http://gdr.openei.org/submissions/1076>, (2018b).
- Energy and Geoscience Institute at the University of Utah: Faults, Fractures, and Lineaments in the Mineral Mountains, Utah [data set]. Retrieved from <http://gdr.openei.org/submissions/713>, (2016).
- Forbes, B., Moore, J., Finnila, A., Podgorney, R., Nadimi, S., and McLennan, J.D.: Natural Fracture Characterization at the Utah FORGE EGS Test Site: Discrete Natural Fracture Network, Stress Field, and Critical Stress Analysis, forthcoming U.S. Geological Survey Bulletin, (2019).
- Golder Associates: FracMan® Reservoir Edition, version 7.7 Discrete Fracture Network Simulator, (2019).
- Gwynn, M., Allis, R., Hardwick, C., Jones, C., Nielsen, P., and Hurlbut, W: Compilation of Rock Properties from Well 58-32, Milford, Utah FORGE Site, FORGE Utah Technical Report, Report to Department of Energy, Geothermal Technologies Office, April 2018, (2018).
- Idaho National Laboratory: Utah FORGE Roosevelt Hot Springs Earth Model Mesh Data for Selected Surfaces [data set]. Retrieved from <http://gdr.openei.org/submissions/1107>, (2018).
- Mauldon, M., and Mauldon, J.G: Fracture sampling on a cylinder: From scanlines to boreholes and tunnels, *Rock Mech. Rock Eng.* **30**(3), (1997), 129-144.
- McLennan, J., Nadimi, S., Trang, T. and Forbes, B.: Permeability Measurements, FORGE Utah Technical Report, Report to Department of Energy, Geothermal Technologies Office, April 2018, (2018).
- Moore, J., McLennan, J., Handwerger, D., Finnila, A., and Forbes, B.: Mechanical Property Measurements, FORGE Utah Technical Report, Report to Department of Energy, Geothermal Technologies Office, April 2018, (2018).
- Sibbett, B.S., and Nielson, D.L.: Geologic map of the central Mineral Mountains, Beaver County, Utah (GIS Reproduction of 1980 Map): Utah Geological Survey, MP-17-2dm, scale 1:24,000 (2017).
- Terzaghi, R.: Sources of Error in Joint Surveys, *Géotechnique*, **15**, (1965), 287-304.